Research Square

Preprints are preliminary reports that have not undergone peer review.
They should not be considered conclusive, used to inform clinical practice,
or referenced by the media as validated information.

Prognostic and immunological significance of an M2 macrophages-related gene signature in cervical cancer

Wenwen Zhang

Zwenwen@whu.edu.cn

Wuhan No.1 Hospital

Min Su

Tangdu Hospital, Air Force Medical University

Ziyan Liang

Zhongnan Hospital of Wuhan University

Yang Gao

Zhongnan Hospital of Wuhan University

Xuemei Gao

Wuhan No.1 Hospital

Liyuan Chen

Wuhan No.1 Hospital

Jie Liu

Zhongnan Hospital of Wuhan University

Yajun Hu

Wuhan No.1 Hospital

Research Article

Keywords: M2 Macrophage-related Genes, Cervical Cancer, Prognostic Model, Immune Microenvironment

Posted Date: November 18th, 2026

DOI: https://doi.org/10.21203/rs.3.rs-11665200/v1

License: This work is licensed under a Creative Commons Attribution 4.0 International License.
Read Full License

Additional Declarations: No competing interests reported.

Prognostic and immunological significance of an M2 macrophages-related gene signature in cervical cancer

Wenwen Zhang[1*], Min Su[2], Ziyan Liang[3], Yang Gao[3], Xuemei Gao[1], Liyuan Chen[1]， Jie Liu[4*]， Yajun Hu[1*]

1. Department of Obstetrics and Gynecology, Wuhan No.1 Hospital, Wuhan, China.
2. Department of Gynecology and obstetrics, Tangdu Hospital, Air Force Medical University, Xian, China.
3. Department of Gynecological Oncology, Zhongnan Hospital of Wuhan University, Wuhan, China.
4. Department of Hepatobiliary and Pancreatic Surgery, Zhongnan Hospital of Wuhan University, Wuhan, China.

*** Corresponding authors:**

Wenwen Zhang, email: zwenwen@whu.edu.cn

Jie Liu, email: liuj_0313@163.com

Yajun Hu, email: whyyy191@sina.com

ABSTRACT

Background

M2 macrophages contribute to cervical cancer progression and immune regulation within the tumor microenvironment. However, the clinical relevance and prognostic value of M2 macrophage-related genes (MRGs) in cervical cancer remain poorly defined.

Methods

Weighted gene co-expression network analysis and Pearson correlation analysis of the TCGA-CESC and GSE44001 datasets identified 63 MRGs, which were subjected to functional enrichment analysis. A two-gene prognostic model was developed using univariate Cox regression, least absolute shrinkage and selection operator regression, and multivariable Cox regression. Patients were stratified into high- and low-risk groups according to the median risk score. Survival outcomes, immune cell infiltration, genomic alterations, and anticancer drug sensitivity were compared between groups. PKD2L1 and PILRA expression in cervical cancer and adjacent normal tissues was assessed using quantitative PCR and western blotting. The effects of gene overexpression on cell proliferation and apoptosis were evaluated using Cell Counting Kit-8, colony formation, and flow cytometry assays. The effects of PKD2L1 and PILRA co-expression on tumorigenicity were evaluated in a subcutaneous xenograft model in nude mice. Intratumoral M2 macrophage distribution was assessed using multiplex immunohistochemistry.

Results

A prognostic model comprising PKD2L1 and PILRA was developed and validated. High-risk patients had significantly poorer survival outcomes than low-risk patients. The risk score remained independently associated with prognosis, and the model showed consistent prognostic performance across clinical subgroups. Gene set enrichment analysis revealed reduced enrichment of immune-related pathways in the high-risk group. CIBERSORT and single-sample gene set enrichment analysis indicated lower immune cell infiltration in this group. High-risk patients also exhibited higher tumor mutational burden and greater genomic instability. Model-derived risk scores were associated with anticancer drug sensitivity. PKD2L1 and PILRA expression was significantly lower in cervical cancer tissues than in adjacent normal tissues. In vitro, overexpression of PKD2L1 and PILRA inhibited cervical cancer cell proliferation, promoted apoptosis, and increased cisplatin sensitivity. In nude mice, overexpression of these genes suppressed xenograft growth and reduced tumor weight. Multiplex immunofluorescence showed that their combined overexpression significantly

reduced intratumoral M2 macrophage infiltration.

Conclusions

The PKD2L1－PILRA prognostic model may support risk stratification and characterize differences in immune infiltration and drug sensitivity in cervical cancer. Functional experiments provide preliminary evidence supporting tumor-suppressive roles for both genes. These findings warrant further investigation of their potential as prognostic biomarkers and therapeutic targets.

Keywords

M2 Macrophage-related Genes, Cervical Cancer, Prognostic Model, Immune Microenvironment

INTRODUCTION

In recent years, significant progress has been made in the early detection and prevention of cervical cancer, largely attributed to the widespread implementation of cervical cancer screening and vaccination programs. However, cervical cancer remains one of the most prevalent malignancies among women globally, with approximately 57,000 new cases and 31,100 deaths reported worldwide in 2018[1-3]. Current therapeutic strategies for cervical cancer include surgery, chemotherapy, radiotherapy, and targeted therapy[4]. Although these approaches have contributed to a reduction in mortality rates, the efficacy of cancer treatment is often limited by the high degree of tumor heterogeneity[5]. Patients with advanced or recurrent cervical cancer have a median survival of approximately 17 months, with a five-year survival rate of only about 17%. Furthermore, the overall prognosis for patients with metastatic cervical cancer remains poor[6].

Accurate prognostic and therapeutic evaluation is essential for guiding treatment decisions in clinical settings. In practice, the histopathological classification and staging system provided by the International Federation of Gynecology and Obstetrics (FIGO) is commonly used to guide cervical cancer treatment strategies and assess patient prognosis. However, patients within the same FIGO stage[7] may exhibit divergent survival outcomes despite receiving identical treatments, highlighting the limitations of current predictive systems and underscoring the complex molecular characteristics and intrinsic heterogeneity of cervical cancer[8]. Consequently, there is an urgent need to develop more robust prognostic models based on the biogenetic features of cervical cancer. Such models would enable personalized treatment management through early risk stratification, ultimately improving survival rates and quality of life for patients with cervical cancer.

The infiltration of immune cells within the tumor immune microenvironment (TME) plays a pivotal role in tumorigenesis, progression, and response to immunotherapy[9]. Among these, macrophages are recognized as the most abundant non-tumor cell type in the TME and are involved in both non-specific and specific immune responses against tumors. Tumor-associated macrophages (TAMs) have been demonstrated to directly or indirectly regulate key features of tumors, including tumor growth, invasion, angiogenesis, immune evasion, and drug resistance[10,11]. TAMs exhibit high plasticity and heterogeneity, and under the influence of various signals within the TME, they can polarize into classically activated macrophages (M1) or alternatively activated macrophages (M2)[12,13]. M1 macrophages can upregulate the expression of interleukin-6 (IL-6) and increase the expression of CD86 and CD80, thereby initiating T-cell responses and exerting anti-tumor effects[14]. In contrast, studies by Wang et al.

have shown that M2 macrophages enhance the reactivity of tumor-associated fibroblasts and promote epithelial-mesenchymal transition (EMT) through the secretion of transforming growth factor-beta (TGF-β), thereby facilitating tumor proliferation and invasion[15]. Furthermore, M2 TAMs contribute to the formation of an immunosuppressive TME by inducing cytotoxic T-cell dysfunction at the tumor site, ultimately mediating tumor immune evasion and resistance to immunotherapy[16,17]. Notably, a high M2/M1 ratio has been identified as a significant prognostic factor in various cancers. Consequently, the molecular characteristics of M2 TAM infiltration may serve as a valuable indicator for predicting the prognosis and therapeutic response of cervical cancer patients. However, directly quantifying macrophage infiltration remains challenging. Therefore, the development of an intuitive and specific predictive tool related to M2 macrophages holds substantial clinical significance for the stratified management and prognostic assessment of cervical cancer patients.

Our study aims to investigate the potential of M2 macrophage-related genes as biomarkers for assessing risk and prognosis in cervical cancer patients. We developed a prognostic risk model based on M2 macrophage-related marker genes and comprehensively evaluated its predictive performance. Additionally, we explored the relationship between this risk model and tumor immune cell infiltration, genetic mutation profiles, and drug sensitivity. These findings reveal the immunogenomic characteristics of cervical cancer and identify potential clinically valuable biomarkers, which may provide guidance for the development of personalized treatment strategies. Furthermore, through in vitro and in vivo experiments, we preliminarily investigated the biological roles of PKD2L1 and PILRA in cervical squamous cell carcinoma (CESC).

Materials and methods

Data collection and pre-processing

The TCGA-CESC dataset, comprising 307 cases, was obtained from the TCGA database (https://portal.gdc.cancer.gov). After excluding patients with missing clinical information, a total of 255 cases were included in the analysis. Gene expression data were acquired by converting FPKM values to TPM values. The GSE44001 dataset, consisting of 300 cases, was retrieved from the GEO database (https://www.ncbi.nlm.nih.gov/geo/). Normalization and differential expression analysis of the TCGA-CESC and GSE44001 datasets were performed using the limma package in R software.

Identification of MRGs Associated with M2 Macrophage Infiltration

The relative abundance of M2 macrophages in the gene expression data was calculated using the CIBERSORTx algorithm[18], and the correlation between MRG expression and M2 macrophage infiltration levels was assessed using Spearman correlation analysis. Weighted gene co-expression network analysis (WGCNA) was employed to identify genes most strongly associated with M2 macrophage content in cervical cancer (CC). Initially, expression data were extracted, missing values were checked, and outliers were removed. An appropriate soft-thresholding power (β) was selected based on the scale-free topology fitting index, and the minimum number of genes per module was set to 50. The "dynamic tree cut" algorithm was used to merge highly similar modules, resulting in the division of all genes into eight distinct modules. Subsequently, the module most correlated with M2 macrophage content was identified using Pearson correlation analysis. Genes from this module were intersected with M2 macrophage-related genes, yielding a refined set of M2-like tumor-associated macrophage (TAM)-related genes.

Functional Enrichment Analysis

We performed functional annotation analysis on M2-like TAM-related genes using the R package "clusterProfiler"[19]. Gene Ontology (GO, http://www.geneontology.org/) enrichment analysis was conducted to categorize genes based on biological processes, cellular components, and molecular functions, while Kyoto Encyclopedia of Genes and Genomes (KEGG, http://www.kegg.jp/kegg/pathway.html) pathway enrichment analysis was employed to identify relevant signaling pathways. The R package "ggplot2" was utilized to visualize the biological functional data of these genes, providing a clear and interpretable representation of their roles and pathways.

Construction and Validation of a M2-like TAM-related prognostic model

To identify M2-like TAM-related genes with prognostic significance for constructing a predictive model, we performed univariate Cox regression analysis. Subsequently, least absolute shrinkage and selection operator (LASSO) regression analysis was applied to further filter out overfitted genes. The R package "glmnet" was utilized to develop an M2-like TAM-related prognostic model. To stratify cervical cancer patients into distinct risk groups, a risk score for each patient was calculated based on gene expression levels and their corresponding regression coefficients using the following formula:

$$risk\ Score = \sum_{i=1}^{n} [coeffecient(genei) * expression(genei)]$$

Subsequently, patients were stratified into low-risk (risk score < median value) or high-risk (risk score > median value) groups based on the median risk score.

The prognostic predictive capacity of the risk model for cervical cancer patients was investigated and validated through Kaplan-Meier survival curves. To demonstrate that the risk score serves as an independent prognostic factor, univariate and multivariate Cox regression analyses were performed using the "survival" R package, incorporating both the risk score and clinical factors. Time-dependent receiver operating characteristic (ROC) curve analysis was conducted using the "survivalROC" R package to evaluate the risk score and clinically independent prognostic factors, with the area under the curve (AUC) values at 1-, 3-, and 5-year intervals used to assess the sensitivity and specificity of the risk score model.

With overall survival (OS) as the primary observational endpoint, a nomogram was developed by incorporating the contributions of predictive variables to the survival risk within the model. The predictive accuracy of the nomogram was subsequently evaluated and validated using calibration curves.

Immune infiltration analysis (CIBERSORT)

Based on the expression matrix of human immune cell subtypes, the CIBERSORT algorithm (https://cibersort.stanford.edu/) was employed to calculate the enrichment scores of 22 immune cell populations. The Kruskal-Wallis test was subsequently applied to assess the correlation between immune cell infiltration and risk scores. To further investigate the differences in immune functional activity between high-risk and low-risk groups, the R packages

"GSEABase" (www.bioconductor.org/packages/release/bioc/html/GSEABase.html/) and "GSVA" were utilized for gene set variation analysis (GSVA), enabling the quantification and comparison of immune functional scores across the two groups.

Mutation landscape and drug sensitivity analysis

The mutation profiles of the two risk groups were visualized using waterfall plots generated by the R package "Maftools". Additionally, the tumor mutation burden (TMB) between the two risk groups was compared using the R packages "ggpubr" and "reshape2". Leveraging drug sensitivity data from the Genomics of Drug Sensitivity in Cancer (GDSC) database (https://www.cancerrxgene.org/), the half-maximal inhibitory concentration (IC50) values for various antitumor drugs were calculated using the R package "oncopredict". Lower IC50 values indicate higher therapeutic efficacy of the drugs against cancer.

Cell culture

The human cervical cancer cell line SiHa and the human renal epithelial cell line HEK293T were obtained from the Cell Bank of the Chinese Academy of Sciences (Shanghai, China). SiHa cells were cultured in DMEM medium supplemented with 10% fetal bovine serum (FBS) and 1% penicillin-streptomycin, while HEK293T cells were maintained in RPMI 1640 medium containing 10% FBS and 1% penicillin-streptomycin. All cells were incubated at 37 °C in a humidified atmosphere with 5% CO2.

The pLenti-PKD2L1, pLenti-PILRA, and pLenti-empty vector plasmids were constructed and transfected into HEK293T cells. After 48 hours of transfection, the lentivirus-containing supernatant was harvested and filtered through a syringe filter. SiHa cells were then incubated with the diluted lentivirus in fresh medium containing 10 ng/mL polybrene for 16 hours. Following transduction, the cells were collected and cultured in medium supplemented with 2.5 ng/mL puromycin. Surviving cells were harvested for subsequent screening and experimental use.

RNA isolation and qRT-PCR enzyme chain reaction

Total RNA was extracted from cells using TRIzol reagent (TaKaRa, Japan). Subsequently, the extracted RNA was reverse-transcribed into cDNA using the Taq Pro Universal SYBR qPCR Master Mix kit (Vazyme, China), followed by quantitative reverse transcription PCR (RT-

qPCR). GAPDH was used as an internal reference gene, and the relative mRNA expression levels of PKD2L1 and PILRA were normalized and compared using the 2-ΔΔCt method. The primer sequences are listed in Table 1.

Tab. 1 Primer sequence

Gene name	Primer sequence
PKD2L1	F 5'- GACTTTGGGGAACAACCCTGA -3'
	R 5'- GGAGCTTGTCATTCCATAGGTCA -3'
PILRA	F 5'-CTGGAGGCTCAGTAGCACAAC -3'
	R 5'- GGAGGCAGATCAGTCCCAAAAT -3'
GAPDH	F 5'-CTGGGCTACACTGAGCACC-3'
	R 5'-AAGTGGTCGTTGAGGGCAATG-3'

Western blotting analysis

Total cellular proteins were extracted using RIPA lysis buffer (Biosharp, China) supplemented with PMSF (Beyotime, China). The cell lysates were separated by 10% SDS-PAGE, and the resolved proteins were transferred onto polyvinylidene fluoride (PVDF) membranes. The membranes were blocked with 5% skim milk (Biosharp, China) at room temperature for 1 hour. Subsequently, the membranes were incubated overnight at 4 °C with primary antibodies against PKD2L1 (13117-2-AP, Proteintech, China), PILRA (11818-1-AP, Proteintech, China), and GAPDH (60004-1-IG, Proteintech, China). After washing three times with TBST, the membranes were incubated with corresponding secondary antibodies at room temperature for 90 minutes. Protein bands were visualized using an ECL detection kit (Vazyme, China), and images were captured using a Tanon multifunctional imaging system (Tanon 5200 Multi, China).

Cell Counting Kit-8 assay

Cells were seeded into 96-well plates at a density of 2 × 10^3 cells per well and cultured at 37 °C. After cell attachment, the culture medium was replaced at 0 h, 24 h, 48 h, 72 h, and 96 h, followed by the addition of 10 μL of CCK-8 solution (Meilune, China) to each well. The plates were then incubated in a 37 °C incubator protected from light for 2 hours. Absorbance at 450 nm was measured using a microplate reader (Bio-Rad, Richmond, CA, USA). For the cisplatin (HY-17394, MCE, USA) treatment experiments, cells were seeded into 96-well plates and cultured for 24 hours, after which cisplatin was added at a concentration of 8 nM. Following the addition of 10 μL of CCK-8 reagent and subsequent incubation, the absorbance was measured as described above.

Colony formation assay

Cells were seeded into six-well plates at a density of 300 cells per well and cultured continuously in a 37 °C incubator for 2-3 weeks. Following incubation, the cells were fixed with 4% paraformaldehyde and stained with 0.5% crystal violet. Colonies were then photographed, and the number of colonies was quantified.

Analysis of apoptosis by flow cytometry

The collected cell pellets, including cells from the culture supernatant, were resuspended in binding buffer. FITC Annexin V and propidium iodide (PI) (Multi Sciences, CHN) were added under light-protected conditions, and the samples were incubated on ice in the dark for 5 minutes. Apoptosis levels in different groups were assessed using flow cytometry, and the acquired data were analyzed using FlowJo software (version 10.6.0).

Evaluation of cervical cancer cell sensitivity assay to cisplatin

To assess the cisplatin resistance of cervical cancer cells, SiHa cells were continuously exposed to cisplatin (HY-17394, MCE, USA) at concentrations ranging from 0 to 32 μM. The half-maximal inhibitory concentration (IC50) was determined by evaluating the number of viable cells adherent to the culture dish at the end of the drug treatment period.

Tumor xenograft studies

SiHa cells stably overexpressing both oe-PKD2L1+PILRA or oe-NC (negative control) were established. Six-week-old female BALB/c-nude mice were purchased from GemPharmatech (China). A cell suspension containing 5 × 10^6 SiHa cells was subcutaneously injected into the right axilla of BALB/c-nude mice. Tumor size was measured every 4 days, and tumor volume was calculated using the formula (width^2 × length)/2. After 20 days, the mice were euthanized, and subcutaneous tumors were harvested for further analysis. The tumor growth curves and final tumor weights were compared between groups. All animal experiments were conducted in accordance with protocols approved by the Institutional Animal Care and Use Committee of zhongnan hospital, Wuhan University.

Multiplexed fluorescence immunohistochemistry

The tumor tissue sections from xenografts were fixed with 4% paraformaldehyde for 30 minutes, followed by permeabilization with 0.1% Triton X-100 at room temperature for 20

minutes. Subsequently, the sections were blocked with 3% bovine serum albumin (BSA) for 60 minutes. Primary antibodies, including anti-F4/80 (29414-1-AP, Proteintech, China) and anti-CD206 (18704-1-AP, Proteintech, China), were applied and incubated overnight at 4°C. Following this, the sections were incubated with corresponding fluorescent secondary antibodies at room temperature for 60 minutes in the dark. Nuclei were counterstained with DAPI for 15 minutes, and images were captured using a fluorescence microscope (Leica).

Statistical analysis

All statistical analyses were performed using R version 4.2.0 and GraphPad Prism 8.0 software, with the R packages for statistical analysis as described above. The Student's t-test and Wilcoxon rank-sum test were employed to assess statistical significance between two groups, while the Kruskal-Wallis test and one-way analysis of variance (ANOVA) were used for comparisons involving more than two groups. Unless otherwise specified, a p-value of <0.05 was considered statistically significant.

RESULTS

1. Construction of WGCNA and identification of M2 macrophage-related genes

To further elucidate the relationship between tumor-associated macrophages (TAMs) and the prognostic survival rates of cervical cancer patients (CCas), we conducted Weighted Gene Co-expression Network Analysis (WGCNA) on the TCGA-CESC and GSE44001 cohorts to identify co-expression modules. The soft-thresholding power for TCGA-CESC was set to 6 (**Fig. 1A**) and for GSE44001 to 5 (**Fig. 1B**), based on the scale-free topology fitting index and mean connectivity. A minimum gene count of 50 per module was established, and genes with similar expression patterns were grouped into the same module using a dynamic tree-cutting algorithm, resulting in a hierarchical clustering tree with distinct modules. Hierarchical clustering analysis was then performed based on weighted correlations, and the clustering results were segmented according to predefined criteria, yielding eight gene modules (MEblack, MEgreen, MEbrown, MEpurple, MEblue, MEmagenta, MEpink, MEgrey). The relationships between genes and their corresponding modules were visualized using dendrograms (**Fig. 1C, D**). In **Fig. 1E** and **F**, each column represents a type of tumor-infiltrating immune cell, while each row corresponds to a candidate module with trait-specific gene vectors. Among the eight candidate modules in the TCGA-CESC cohort, the magenta module exhibited the strongest correlation with M2 macrophages (Cor = 0.62, p = 7e−21, **Fig. 1E**). Similarly, in the GSE44001 cohort, the green module showed the strongest positive correlation with M2 macrophages (Cor = 0.8, p = 3e−24, **Fig. 1F**). Given our primary focus on M2 macrophages, we extracted the genes from the magenta and green modules for further investigation.

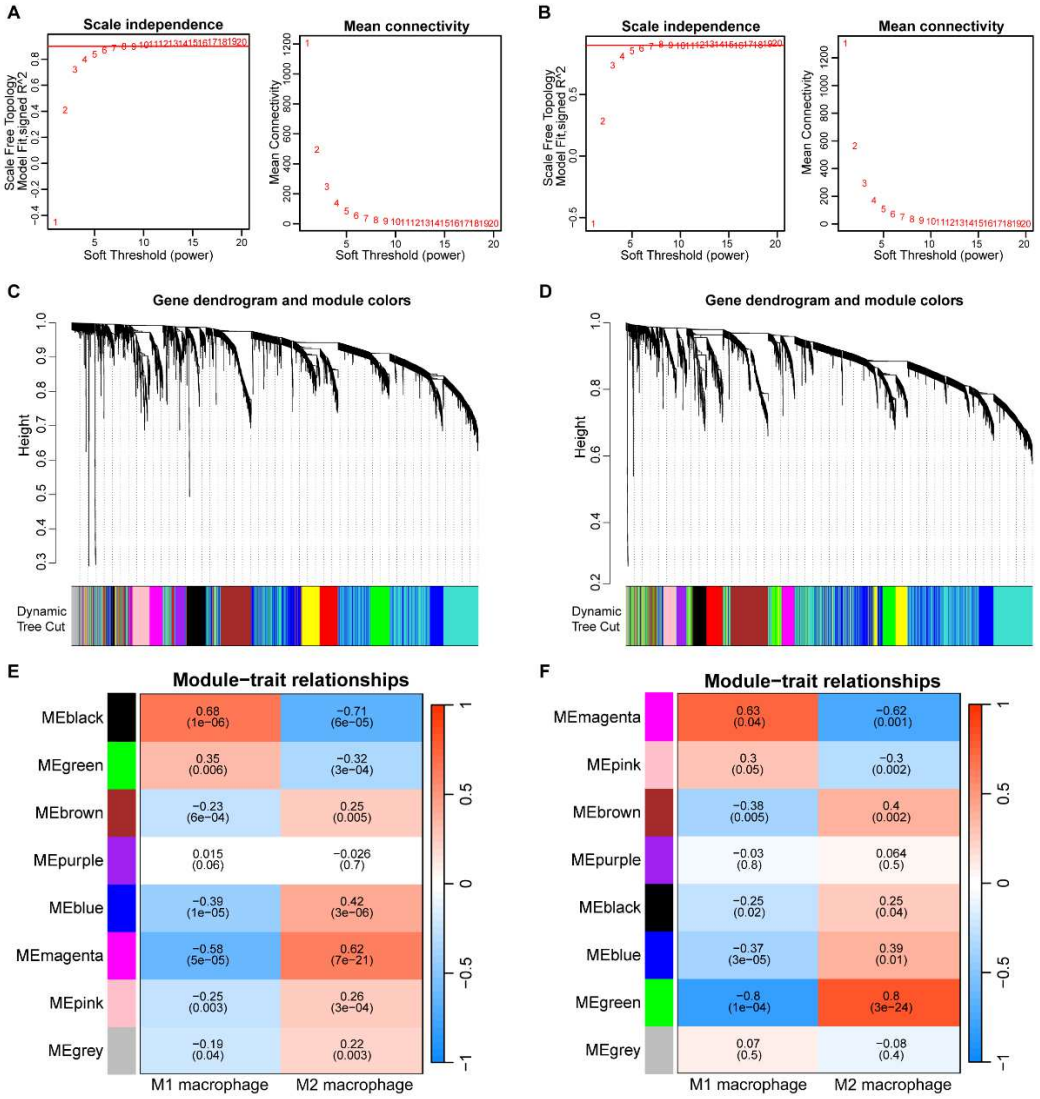


Figure 1. Construction of WGCNA and Identification of M2 Macrophage-Associated Genes

A, B. Determination of the optimal soft threshold power for TCGA-CESC (A) and GSE44001 (B) based on scale independence and mean connectivity. **C, D.** Hierarchical clustering dendrograms illustrate the similarity in expression patterns of genes grouped into co-expression modules in TCGA-CESC (C) and GSE44001 (D). **E, F.** Heatmaps depict the correlation and statistical significance between modules and M1/M2 macrophages. In TCGA-CESC (E), the magenta module, and in GSE44001 (F), the green module, were identified as the modules most strongly associated with M2 macrophages.

2. Identification of M2 Macrophage-Associated Genes

Through WGCNA analysis, we identified 585 genes from the green module in GSE44001 and 497 genes from the magenta module in TCGA-CESC. Using CIBERSORT and Spearman

correlation analysis, we further obtained 427 genes associated with M2 macrophages. By intersecting these datasets and employing Venn diagram analysis, we screened and identified 63 candidate M2-like macrophage-related genes (MRGs). To explore the correlation between co-expressed genes from the TCGA-CESC and GSE44001 datasets and the infiltration abundance of M2 macrophages, we constructed a co-expression network for visualization. The results demonstrated that all 63 MRGs were positively correlated with M2 macrophage infiltration (cor > 0.1, $p < 0.05$) (**Fig. 2A, B**). A heatmap displayed the top 30 correlated MRGs, including VSIG4, CD163, MS4A4A, HK3, and others (**Fig. 2C**). Subsequently, we performed Gene Ontology (GO) and Kyoto Encyclopedia of Genes and Genomes (KEGG) pathway analyses to investigate the molecular characteristics of the 63 M2 macrophage-related MRGs. KEGG pathway enrichment analysis revealed that these MRGs were primarily involved in regulating the JAK-STAT signaling pathway, phagosome formation, Toll-like receptor signaling pathway, and NF-κB signaling pathway, among others (**Fig. 2D**). GO enrichment analysis (**Fig. 2E**) indicated that, in terms of biological processes (BP), the MRGs were mainly associated with myeloid leukocyte activation, immune response-regulating signaling pathways, phagocytosis, and myeloid leukocyte migration. For cellular components (CCs), they were predominantly linked to secretory granule membranes, the external side of the plasma membrane, and tertiary granule membranes. In molecular functions (MF), immune receptor activity, cargo receptor activity, and immune receptor binding were the most prominent features. These findings suggest that the influence of MRGs on M2 macrophage infiltration in cervical cancer may be mediated through their involvement in regulating the aforementioned signaling pathways and biological processes.

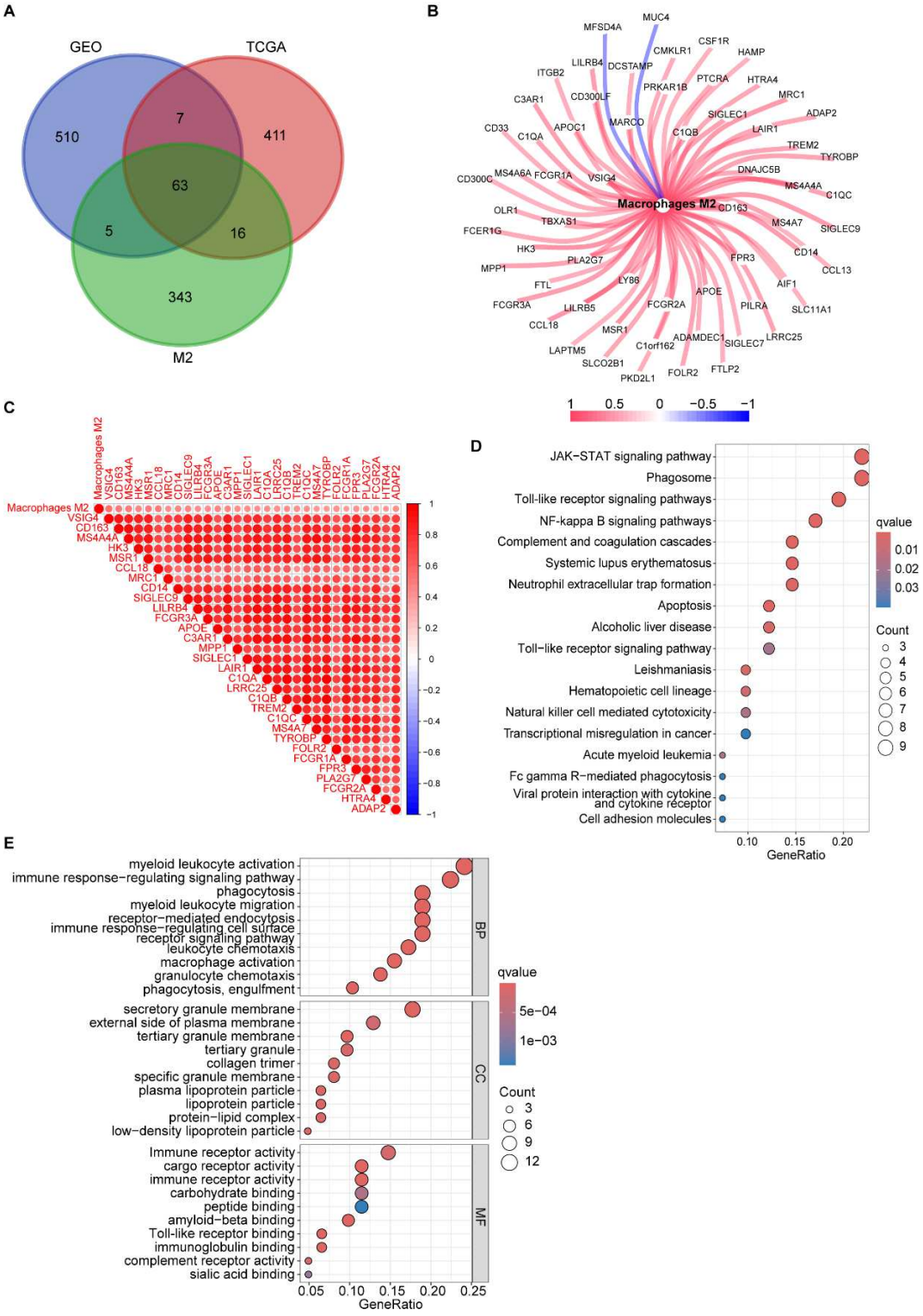


Figure 2. Identification of M2 Macrophage-Associated Genes

A. Venn diagram illustrating the overlap between M2 macrophage-associated module genes derived from TCGA and GEO datasets and M2-related genes identified through Pearson correlation analysis. **B.** Heatmap of M2 macrophage-associated genes. The color gradient represents the magnitude of the correlation coefficients. **C.** Correlation heatmap of selected M2

macrophage-associated genes, highlighting their respective correlation coefficients. **D.** KEGG pathway enrichment analysis of M2 macrophage-associated genes, revealing significant biological pathways. **E.** Gene Ontology (GO) enrichment analysis of M2 macrophage-associated genes, detailing their functional annotations and biological processes.

3. Construction of a Risk Prognostic Model Based on M2 Macrophage-Related Genes

To evaluate the prognostic significance of MRGs associated with M2 macrophage infiltration in cervical cancer, we constructed a prognostic model based on 63 MRGs. The TCGA-CESC cohort (comprising 306 samples) was utilized as the training set, while the GSE44001 cohort (including 300 samples) served as the validation set. Univariate Cox regression analysis was employed to assess the correlation between MRG expression levels and overall survival (OS) in cervical cancer patients, identifying 12 MRGs significantly associated with OS (OS-MRGs), which were subsequently recognized as potential prognostic targets (**Fig. 3A**). Next, we performed LASSO regression with cross-validation to further refine the training set by filtering out overfitted genes (**Fig. 3B, C**). This process yielded a prognostic gene signature comprising two MRGs, PKD2L1 and PILRA, which were strongly associated with OS. The risk score for each patient was calculated using the coefficients of the M2 macrophage-related genes, with the formula for risk score determination as follows:

$$risk\ Score = \sum_{i=1}^{n} [coeffecient(genei) * expression(genei)]$$

Based on the median risk score, samples were stratified into low-risk (L-R) and high-risk (H-R) groups (**Fig. 3D**). The distribution of survival times revealed that higher risk scores were associated with an increased incidence of mortality events (**Fig. 3E**). Kaplan-Meier survival analysis demonstrated that, in the training set, patients in the H-R group had significantly shorter overall survival (OS) compared to those in the L-R group ($P < 0.001$, **Fig. 3D**). Similarly, in the validation set, the L-R group exhibited significantly better prognosis than the H-R group ($P < 0.001$, **Fig. 3E**), confirming the robust predictive performance and broad applicability of the prognostic model. Furthermore, to evaluate the independence of the MRG-based risk score from other clinical factors, univariate and multivariate Cox proportional hazards regression analyses were performed. Univariate Cox analysis revealed that the risk score was significantly associated with OS (HR = 2.715, 95% CI = 1.216–6.061, $p = 0.015$) (**Fig. 3F**). After adjusting for potential confounding variables, multivariate Cox analysis confirmed that the risk score remained an independent predictor of OS (HR = 3.987, 95% CI = 1.350–6.610, $p = 0.007$) (**Fig. 3G**). In summary, these findings demonstrate that the MRG-based risk prognostic model

exhibits strong predictive capability for cervical cancer prognosis.

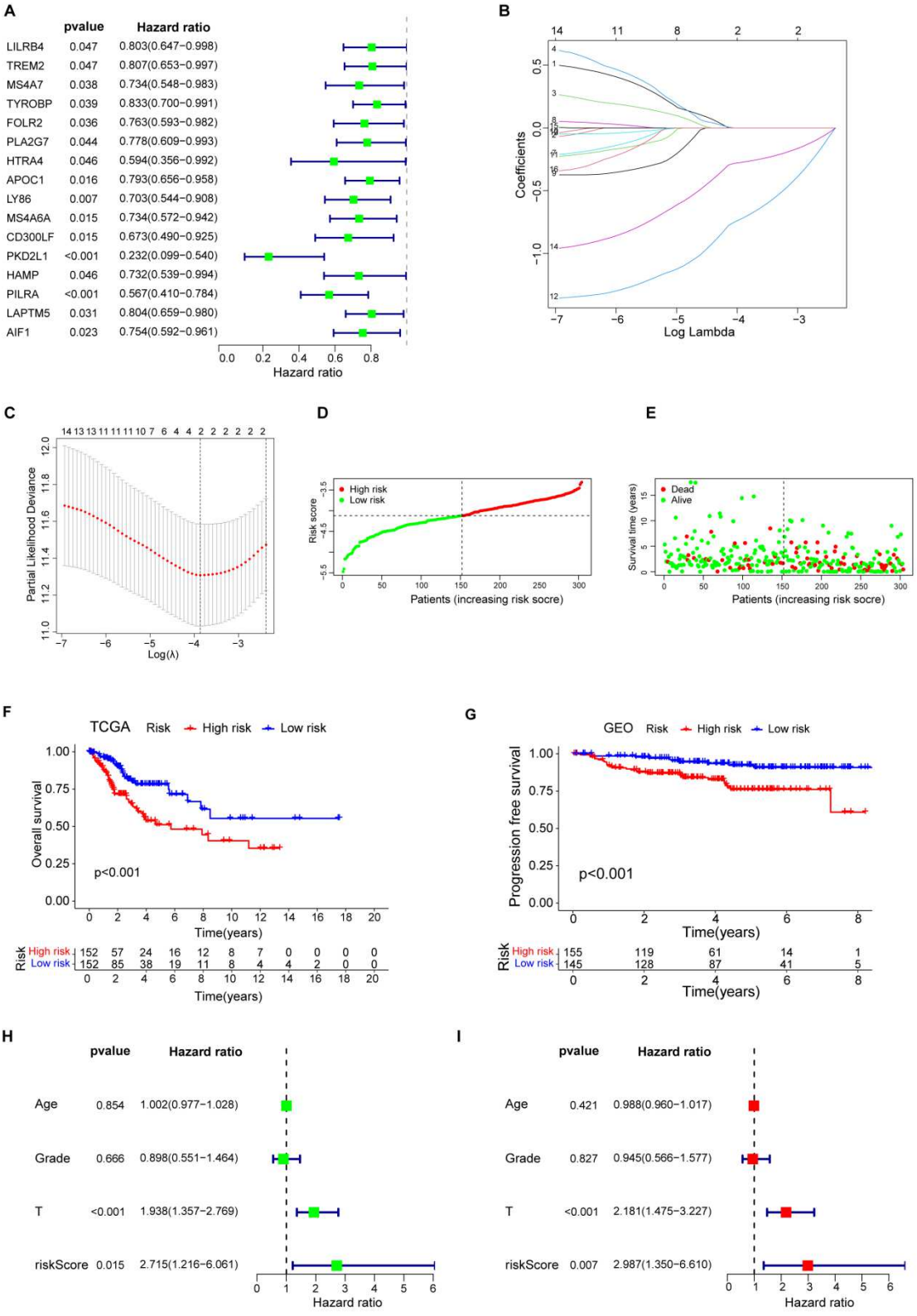


Figure 3. Construction of a Risk Prognostic Model Based on M2 Macrophage-Related Genes

A. Univariate Cox regression analysis identified M2 macrophage-related prognostic genes.

B. LASSO regression analysis of M2 macrophage-related prognostic genes. **C.** Optimal penalty coefficient in the LASSO regression model. **D, E.** Risk score distribution (H) and survival status (I) of high-risk and low-risk groups in the TCGA cohort. **F.** Overall survival analysis of high-risk and low-risk groups in the TCGA cohort, as assessed by the prognostic model. **G.** Progression-free survival analysis of high-risk and low-risk groups in the GEO cohort (GSE44001), as evaluated by the prognostic model. **H, I.** Forest plots illustrating the independent prognostic value of the risk score based on univariate Cox regression (F) and multivariate Cox regression (G) analyses in the TCGA cohort.

4. Validation of the Prognostic Model

To further assess the performance of the prognostic model, we constructed time-dependent receiver operating characteristic (ROC) curves. The area under the curve (AUC) values for 1-year, 3-year, and 5-year overall survival (OS) were 0.710, 0.645, and 0.681, respectively (**Fig. 4A**). Additionally, we compared the 5-year AUC values of age, pathological stage, and risk score. The results demonstrated that the AUC value of the risk score was higher than those of age and pathological stage, indicating that the MRG-based risk score exhibits high accuracy in prognostic prediction (**Fig. 4B**). To provide a quantitative tool for potential future clinical evaluation, we developed a nomogram incorporating age, risk score, tumor grade, and other factors to predict patient OS (**Fig. 4C**). The calibration curves for 1-year, 3-year, and 5-year OS closely aligned with the ideal diagonal line, confirming the reliability and accuracy of the model in predicting the prognosis of cervical squamous cell carcinoma (CESC) patients (**Fig. 4D**). Furthermore, we plotted progression-free survival (PFS) Kaplan-Meier curves, corresponding calibration curves, and AUC curves (**Fig. S1**), which demonstrated that the model also has strong predictive value for PFS in cervical cancer patients.

Next, to evaluate whether the risk score model possesses prognostic value independent of clinical features, we performed stratified survival analysis by dividing cervical cancer (CCa) patients into subgroups based on clinical characteristics. Using the risk score model, we further stratified patients aged >60 or ≤60 years (**Fig. 4E**), those with G1-2 or G3-4 grade tumors (**Fig. 4F**), and those with T1-2 or T3-4 stage disease (**Fig. 4G**) into high-risk and low-risk groups. Significant differences in survival outcomes were observed between the groups, indicating that our prognostic model retains robust predictive performance across different clinical strata. Finally, we conducted a combined survival analysis incorporating the risk score and clinically significant prognostic factors. The results revealed that low-risk patients aged ≤60 years and those with early grade had the most favorable prognosis, whereas high-risk patients aged >60 years and those with advanced pathological stages had the poorest outcomes (**Fig. 4H, I**). These

findings demonstrate that our model performs well in predicting the prognosis of cervical cancer patients with diverse clinical variables.

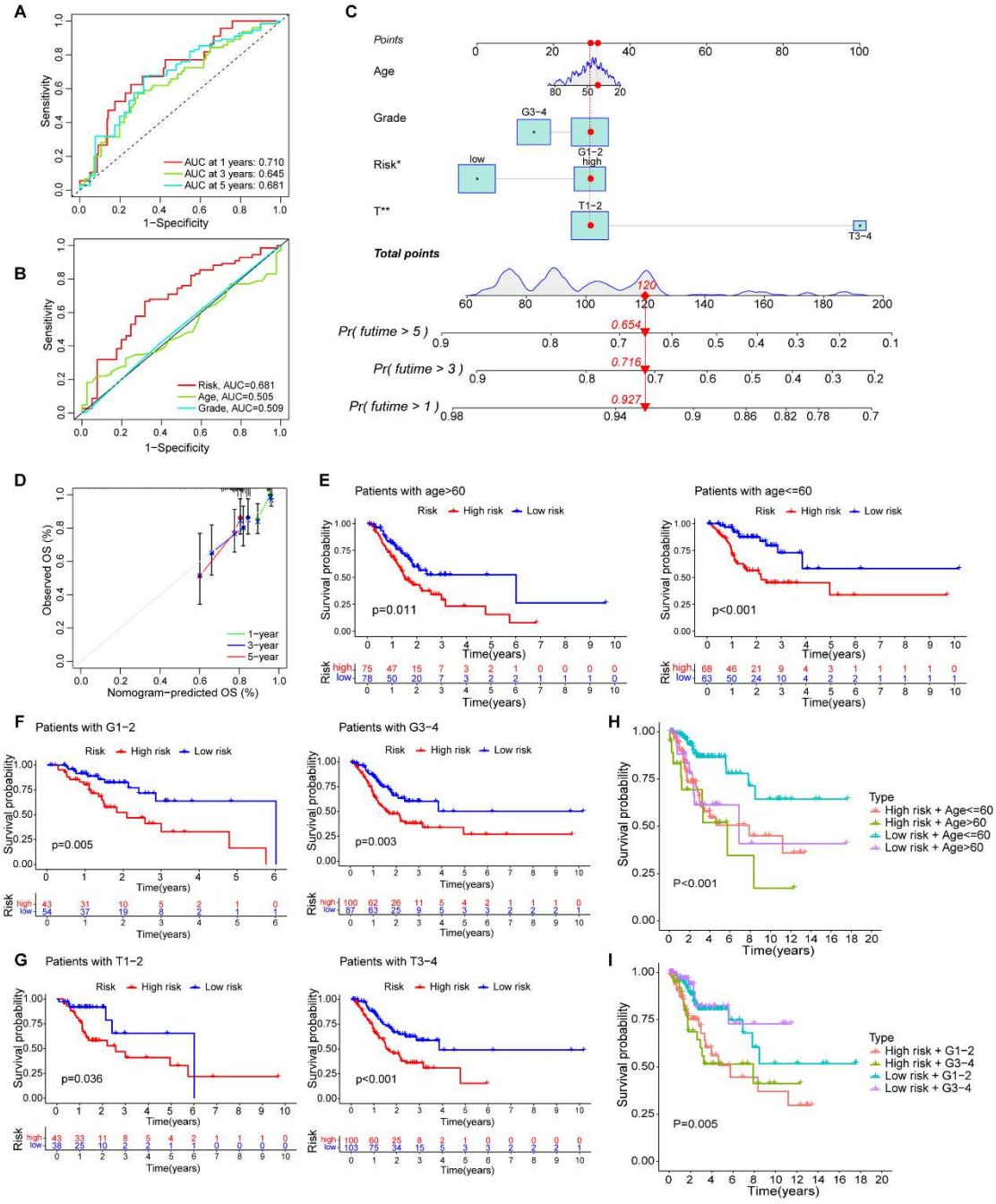


Figure 4. Validation of the Prognostic Model

A. ROC curves of the risk score model for 1-year, 3-year, and 5-year overall survival. **B.** ROC curves comparing the prognostic model and clinical characteristics. **C.** Nomogram for predicting the prognosis of cervical cancer patients in the TCGA cohort. **D.** Calibration curves of the nomogram for 1-year, 3-year, and 5-year survival. **E.** Survival curves stratified by age (≤60 years vs. >60 years). **F.** Survival curves stratified by grade stage (G1-2 vs. G3-4). **G.** Survival curves stratified by T stage (T1-2 vs. T3-4). **H.** Survival curves stratified by high-

risk and low-risk groups in combination with age (≤60 years vs. >60 years). **I.** Survival curves stratified by high-risk and low-risk groups in combination with grade stage (G1-2 vs. G3-4).

5. GSEA analysis between high- and low-risk groups

To investigate the potential mechanisms underlying the differential prognosis between the high- and low-risk groups, we performed Gene Set Enrichment Analysis (GSEA) on the differentially expressed genes between these groups. The results revealed that immune-related pathways were significantly downregulated in the high-risk group, including pathways associated with the T-cell receptor complex, immunoglobulin complex, and antigen binding (**Fig. 5**). These findings suggest that immune cell infiltration may play a critical role in the observed survival differences between the subgroups.

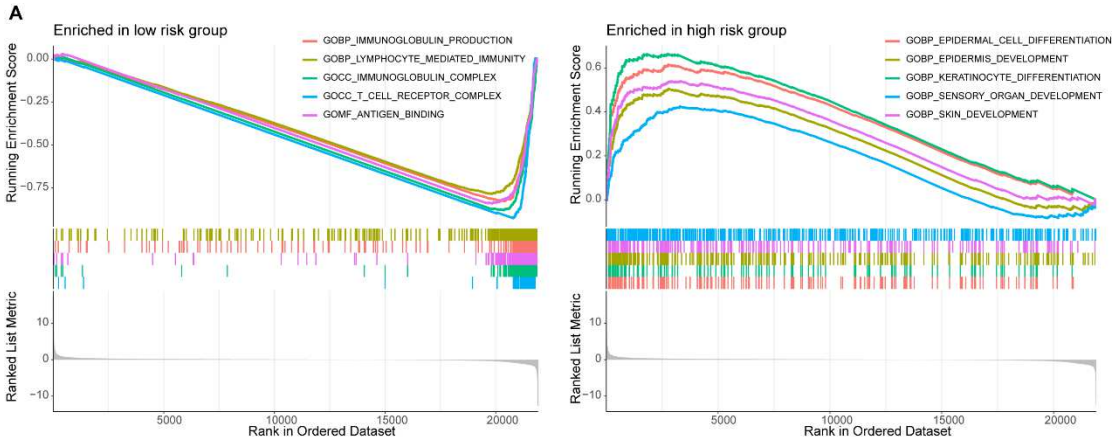


Figure 5. GSEA analysis between high- and low-risk groups.

Gene Set Enrichment Analysis (GSEA) of differentially expressed genes between high- and low-risk groups.

6. Immune Infiltration Analysis of the Risk Prediction Model

Studies have demonstrated that immune cell infiltration within the tumor microenvironment influences host-tumor interactions, playing a pivotal role in tumor progression, therapeutic response, and serving as a critical prognostic factor in cancer[20]. To further explore the relationship between risk scores and immune cell infiltration, we employed the CIBERSORT algorithm to compare the differential expression of 22 immune cell types between the two risk groups in cervical cancer patients. Among the 22 immune cell types, significant differences were observed in plasma cells, CD8+ T cells, activated memory CD4+ T cells, follicular helper T cells, gamma delta T cells, resting dendritic cells, and activated mast cells, with most immune cell types exhibiting lower abundance in the high-risk (H-R) group (**Fig. 6A**). Functional

analysis of immune activity using the ssGSEA algorithm revealed that the low-risk (L-R) group exhibited heightened activity in multiple immune functions, including CD8+ T cells, helper T cells, MHC class I molecules, NK cells, APC co-stimulation, and type II interferon response (**Fig. 6B**). Furthermore, heatmap analysis demonstrated significant differences in immune cell functions across groups stratified by risk score ($p < 0.05$), pathological grade ($p < 0.05$), and clinical stage ($p < 0.001$) (**Fig. 6C**). In summary, our findings suggest a correlation between risk scores and immune response in cervical cancer patients.

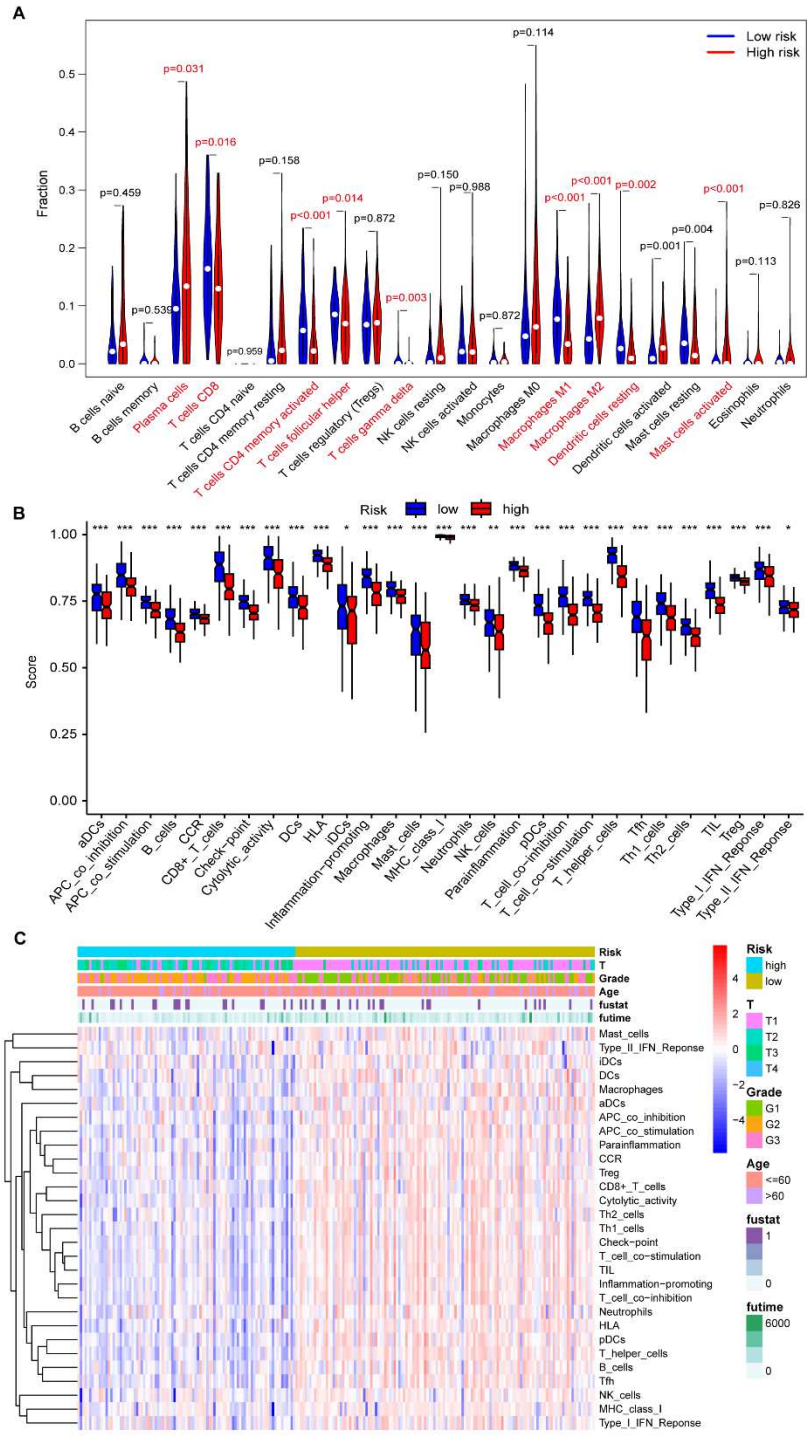


Figure 6. Immune Infiltration Analysis of the Risk Prediction Model

A. Violin plots illustrating the differences in immune infiltration rates of 22 immune cell types between the high- and low-risk groups. **B.** Functional analysis of immune activity using the ssGSEA algorithm, highlighting differences between the high- and low-risk groups. **C.** Heatmap displaying the distribution of ssGSEA scores for immune infiltration, stratified by risk score and clinical characteristics.

7. Gene Mutation and Drug Sensitivity Analysis

Given the profound impact of tumor genomic heterogeneity on the immune microenvironment[21], we compared the frequency and distribution of gene mutations between the two risk groups. Waterfall plots illustrate the top 20 most frequently mutated genes in the cervical cancer cohort (**Fig. 7A, B**). In the high-risk (H-R) group, the top five mutated genes were PIK3CA (29%), TTN (22%), KMT2C (17%), MUC16 (17%), and KMT2D (14%) (**Fig. 7A**), while in the low-risk (L-R) group, the top five mutated genes were TTN (37%), PIK3CA (27%), KMT2C (20%), MUC16 (17%), and FLG (16%) (**Fig. 7B**). Analysis of tumor mutational burden (TMB) revealed that TMB values were significantly higher in high-risk samples compared to low-risk samples ($p < 0.05$) (**Fig. 7C**).

Studies have shown that immune checkpoint genes can suppress the activation of specific immune cells, facilitating tumor immune escape, and blockade of immune checkpoints is considered one of the most effective immunotherapeutic strategies[22]. We investigated the potential association between risk scores and the expression levels of immune checkpoint genes and found that the expression levels of eight immune checkpoint genes, including ATIC, OLA1, CTLA4, PDCD1 (PD-1), CD274 (PD-L1), IDO1, HAVCR2, and PDCD1LG2, were significantly positively correlated with patient risk scores (**Fig. 7D**). These findings provide a theoretical basis for the application of immunotherapy in cervical cancer.

To further explore the potential clinical value of the prognostic model, we assessed the differences in sensitivity to several antitumor drugs between the different subgroups. The lower IC50 values for cisplatin, paclitaxel, topotecan, docetaxel, 5-fluorouracil, gemcitabine, and cyclophosphamide in the low-risk group suggest that this subgroup exhibits lower sensitivity to these chemotherapeutic agents. In contrast, the high-risk group demonstrated lower IC50 values for vincristine and olaparib, indicating that high-risk patients may be more sensitive to these drugs (**Fig. 8**). These findings suggest that our risk model holds significant potential for estimating drug-response petterns and warrants evaluation as a hypothesis-generating tool.

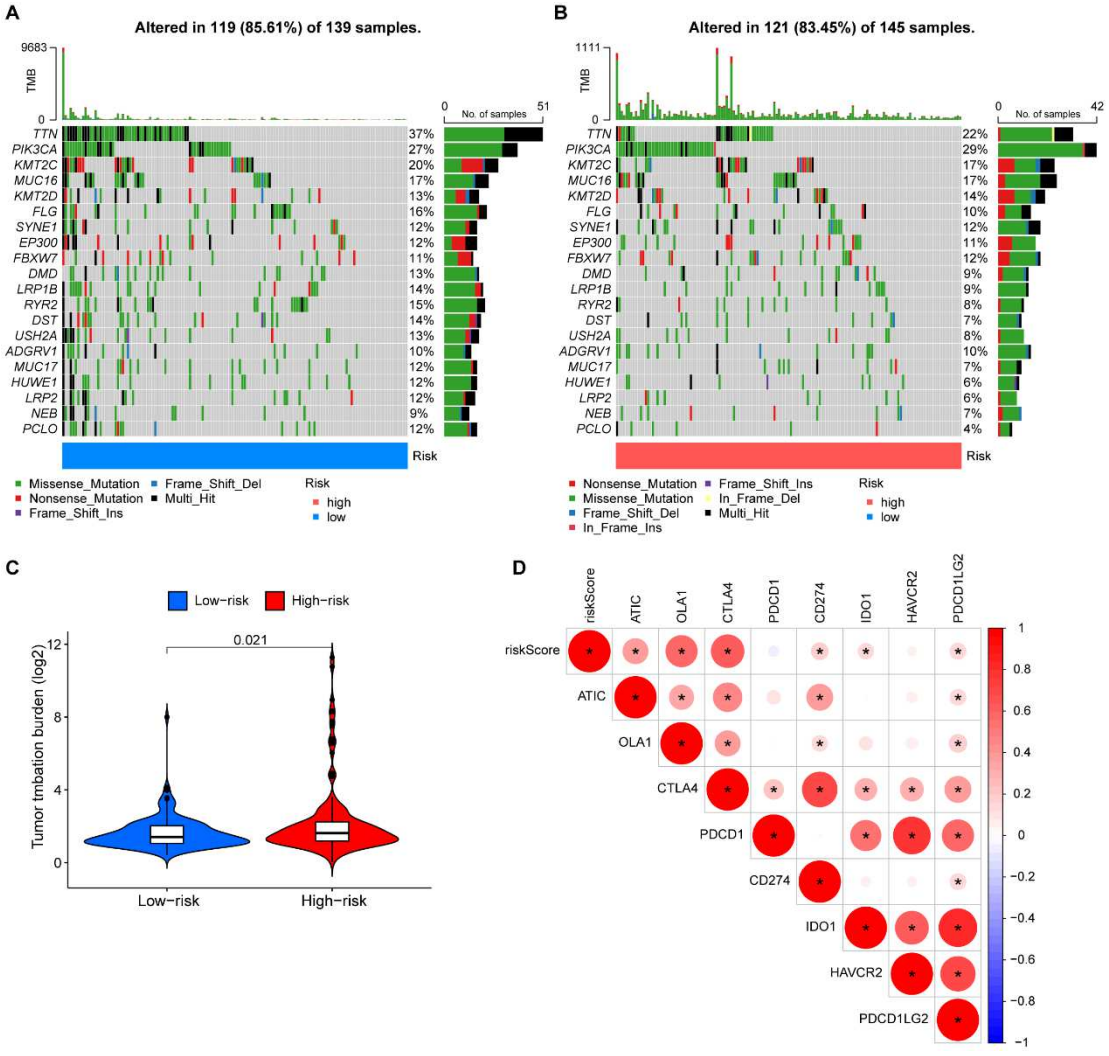
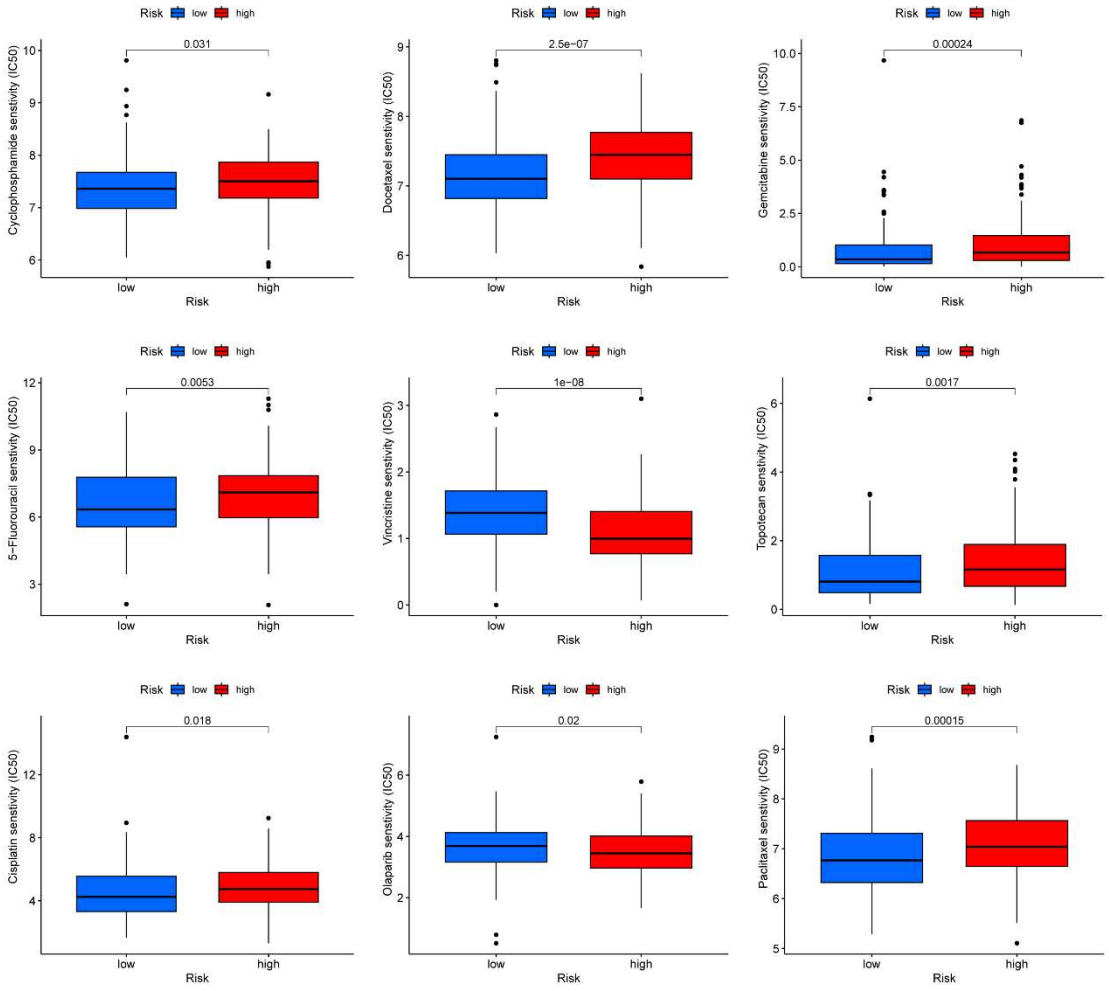


Figure 7. Gene Mutation Analysis

A, B. Waterfall plots illustrate the top 20 mutated genes in high- and low-risk populations. **C.** Violin plots demonstrate the differences in tumor mutation burden (TMB) between high- and low-risk groups. **D.** Correlation analysis between risk scores and immune checkpoint expression.



525

526 **Figure 8. Drug Sensitivity Analysis**

527 Box plots illustrate the mean differences in estimated IC50 values of nine representative
528 antitumor agents (cyclophosphamide, docetaxel, gemcitabine, 5-fluorouracil, vincristine,
529 topotecan, cisplatin, olaparib, and paclitaxel) between the two risk groups.

530

531 **8. PKD2L1 and PILRA Inhibit Cervical Cancer Cell Progression and Enhance Cisplatin**
532 **Sensitivity**

533 To further investigate the roles of PKD2L1 and PILRA, which constitute the predictive model,
534 in cervical cancer, we examined their expression in cervical cancer samples collected from our
535 center. qPCR and Western blot analyses revealed that the expression
536 of PKD2L1 and PILRA was significantly downregulated in tumor tissues compared to normal
537 cervical tissues (**Fig. 9A, B**). We then overexpressed PKD2L1 and PILRA individually in the
538 cervical cancer cell line SiHa and validated the overexpression at both transcriptional and
539 protein levels. The results demonstrated that the overexpression plasmids effectively

upregulated their mRNA and protein levels (**Fig. 9C-E**). CCK-8 and colony formation assays showed that overexpression of PKD2L1 and PILRA significantly inhibited the proliferative capacity of cervical cancer cells, with simultaneous overexpression of both genes further suppressing cell proliferation (**Fig. 9F, G**). Flow cytometry analysis indicated that overexpression of PKD2L1 and PILRA promoted tumor cell apoptosis, and co-overexpression of both genes synergistically enhanced this effect (**Fig. 9H**). Additionally, we observed significant cisplatin resistance in high-risk patients (**Fig. 8**), underscoring the importance of understanding the underlying mechanisms of drug resistance. Our findings revealed that simultaneous overexpression of PKD2L1 and PILRA markedly reduced the IC50 value of cisplatin in CESC cells, indicating increased drug sensitivity (**Fig. 9I**). Moreover, overexpression of PKD2L1 and PILRA enhanced the inhibitory effect of cisplatin on CESC cell proliferation (**Fig. 9J**), suggesting that overexpression of these genes may improve cisplatin sensitivity.

To further explore the impact of PKD2L1 and PILRA on tumor cells in vivo, we subcutaneously inoculated SiHa cells co-overexpressing PKD2L1 and PILRA into nude mice. After 20 days of continuous observation, we found that overexpression of PKD2L1 and PILRA significantly suppressed tumor growth rate and weight (**Fig. 9K-M**). Multicolor immunohistochemistry (mIHC) of the subcutaneous tumors revealed a notable reduction in M2-type macrophages in tumors overexpressing PKD2L1 and PILRA (**Fig. 9N**), suggesting that these genes may inhibit the infiltration of M2-type macrophages into tumor tissues. In summary, our findings provide evidence for the tumor-suppressive roles of PKD2L1 and PILRA in cervical cancer progression. Further investigation into the underlying mechanisms of PKD2L1 and PILRA may offer insights for improving the prognosis of cervical cancer patients.

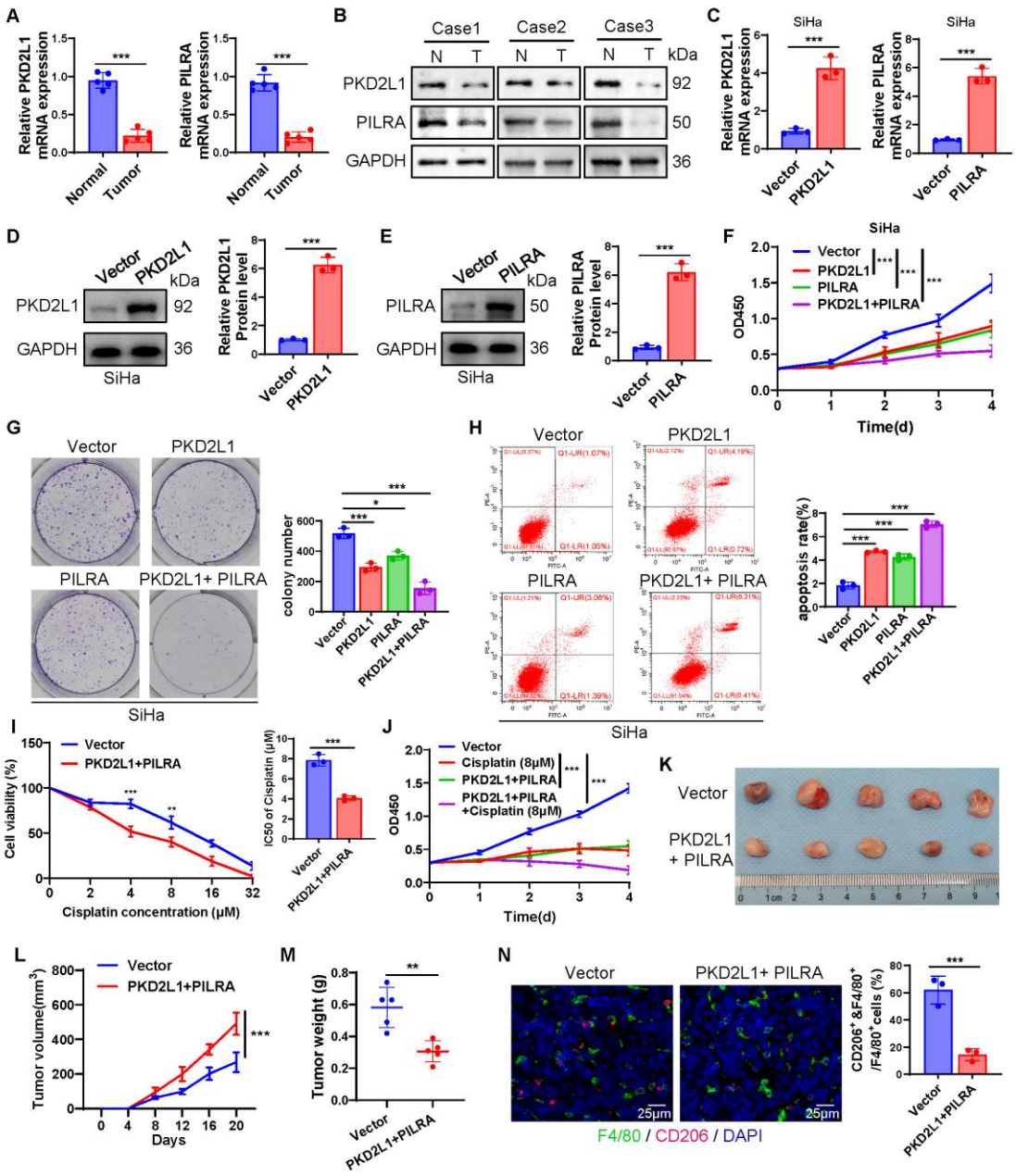


Figure 9. PKD2L1 and PILRA Inhibit Cervical Cancer Cell Progression and Enhance Cisplatin Sensitivity

(A, B) mRNA (A) and protein (B) expression levels of PKD2L1 and PILRA in cervical cancer tissues and normal cervical tissues. (C) qPCR analysis of PKD2L1 and PILRA mRNA expression in SiHa cells transfected with PKD2L1 and PILRA overexpression plasmids or empty vector. (D, E) Western blot analysis of PKD2L1 and PILRA protein levels in overexpression and control cells. (F) CCK-8 assay to assess the proliferative capacity of cells overexpressing PKD2L1, PILRA, or both. (G) Representative images and statistical analysis of colony formation assays. (H) Flow cytometry analysis of apoptosis rates in cells overexpressing PKD2L1 and PILRA. (I) Cell viability and IC50 values of PKD2L1- and PILRA-overexpressing SiHa cells treated with varying concentrations of cisplatin. (J) Impact of

PKD2L1 and PILRA overexpression on cisplatin-induced cytotoxicity in cervical cancer cells. (K) Representative images of subcutaneous tumors at the experimental endpoint. (L) Tumor growth curves based on tumor volume measurements taken every 4 days. (M) Weight of excised subcutaneous tumors at the experimental endpoint. (N) Multiplex immunofluorescence staining and statistical analysis of M2-type macrophages (F4/80+CD206+) in subcutaneous tumors. Scale bar, 25 μm. *$p < 0.05$, **$p < 0.01$, ***$p < 0.001$.

Discussion

Cervical cancer is an immunogenic malignancy characterized by high heterogeneity and metastatic potential, which confers unique immunological features and diversity in its pathogenesis and treatment[3]. Despite ongoing efforts to develop models for accurately predicting the prognosis of cervical cancer patients, the high degree of tumor heterogeneity has often led to suboptimal outcomes. Therefore, integrating high-throughput omics technologies with clinical data to deepen the understanding of the immune characteristics and tumor microenvironment of cervical cancer, as well as to develop more refined and personalized prognostic tools, represents a critical direction for future research.

In recent years, significant progress has been made in the field of tumor molecular medicine, particularly in targeted therapies and immunotherapies. Immune checkpoint blockade (ICB) therapies, such as those targeting programmed cell death protein 1 (PD-1) and cytotoxic T-lymphocyte-associated antigen 4 (CTLA-4), have demonstrated promising therapeutic outcomes in various cancers by activating and enhancing immune responses[23,24]. However, the response rate of cervical cancer patients to existing ICB therapies remains unsatisfactory, ranging from only 4% to 26.3%. This limited efficacy can largely be attributed to the heterogeneity of the tumor and its immune microenvironment, as well as the reliance on the presence of cytotoxic T cells capable of effectively eradicating tumor cells [6,25-27]. Furthermore, against the backdrop of chemotherapy, targeted therapy, and immunotherapy, the issue of drug resistance poses a significant challenge to clinical efficacy[28]. Studies by Wan et al. have demonstrated that the PGEM/PF complex, which activates the STING signaling pathway, can significantly induce antitumor immunity and reduce tumor burden in pancreatic cancer by reversing CCL2/CCL7-mediated immune suppression. Additionally, this complex enhances tumor sensitivity to anti-PD-L1 therapy, achieving complete tumor suppression[29]. These findings suggest that combination therapies offer a promising solution to overcome drug resistance and improve therapeutic outcomes. At the same time, they underscore the urgent need for in-depth research into the mechanisms of immune remodeling in cervical cancer and the exploration of novel therapeutic targets. By understanding and intervening in these mechanisms, we may improve treatment response rates in cervical cancer patients and lay the foundation for the development of personalized therapeutic strategies.

A substantial body of evidence underscores the pivotal role of M2 macrophages in tumor progression and immunosuppression, making the regulation of tumor-associated macrophage (TAM) polarization a critical focus in cancer immunology research. Previous studies have demonstrated that M2 macrophages promote the initiation and metastasis of gallbladder cancer

by secreting copious amounts of chemokine ligand 2 (CCL2), which activates the ERK pathway, leading to poor prognosis[30]. Li et al. revealed that tumor-secreted cathepsin K (CTSK) stimulates M2 polarization of TAMs via the mTOR-dependent pathway, thereby facilitating colorectal cancer metastasis and adverse outcomes[31]. In cervical cancer, Oct4 has been shown to drive tumor metastasis by promoting M2 macrophage polarization[32]. However, compared to other solid tumors, our understanding of M2 macrophages and their specific biomarkers in cervical cancer remains limited. Although related studies have been conducted using existing datasets, prior work has not focused on exploring the relationship between M2 macrophage infiltration and gene expression profiles in cervical cancer. In our study, we successfully identified two M2 macrophage-related marker genes associated with prognosis and constructed a risk prediction model for cervical cancer. Our analysis revealed that the presence of M2 TAMs is significantly correlated with reduced survival rates in cervical cancer patients, and a high-risk score indicates poor prognosis, consistent with previous findings. Furthermore, our model demonstrated robust prognostic predictive performance in both training and validation cohorts, with risk stratification showing strong concordance with clinical staging in prognostic assessment. Univariate and multivariate Cox analyses further confirmed the risk score as an independent prognostic predictor for cervical cancer. In summary, this study provides novel transcriptomic-level insights into the role of M2 macrophages in cervical cancer, identifies potential M2 macrophage-related biomarkers, and offers valuable information for future therapeutic strategies. These findings not only enhance our understanding of the tumor microenvironment in cervical cancer but also provide a critical theoretical foundation for potential future clinical evaluation.

In this study, we observed a reduction in the activity of immune activation-related pathways in the high-risk group. By analyzing the infiltration levels of various immune cells across different subgroups, we uncovered distinct immune infiltration characteristics unique to each subgroup. Among the 22 immune cell types examined, the high-risk group exhibited significantly higher proportions of plasma cells, M2 macrophages, and activated mast cells compared to the low-risk group ($p < 0.05$), whereas the latter demonstrated elevated levels of CD8+ T cells, activated memory CD4+ T cells, γδ T cells, M1 macrophages, and resting dendritic cells ($p < 0.05$) (**Figure 6, A**). Furthermore, immune function analysis revealed that the low-risk group displayed significantly greater activity in CD8+ T cells, helper T cells, MHC class I molecules, NK cells, APC co-stimulation, and type II interferon responses compared to the high-risk group (**Figure 6, B**). These findings indicate that our risk signature not only effectively predicts the prognosis of cervical cancer patients but also exhibits a significant correlation with the immune landscape and immune responses in cervical cancer. Immune cells within the tumor microenvironment (TME) have been extensively studied in various cancers. For instance, γδ T

cells are more abundant in cervical cancer tissues than in normal cervical tissues, and their infiltration levels are positively correlated with patient prognosis. These cells exert direct anti-tumor effects by enhancing the expression of cytotoxicity-related genes[33]. In contrast, most neoantigen-reactive CD8+ T cells in the TME are functionally impaired or exhausted, with only a minority retaining effective immune functionality[34,35]. Cherdantseva et al. suggested that mast cell infiltration indicates poor prognosis in muscle-invasive bladder cancer[36]. Interestingly, further analysis revealed that the expression levels of immune checkpoint genes in patients were positively correlated with our risk score. Indeed, immune checkpoint proteins can induce T cell exhaustion, interfere with cytotoxic T cell targeting of tumor cells, and facilitate immune escape of tumor cells[37,38]. It is evident that the high-risk group is associated with reduced immune cell infiltration and weaker immune responses, reflecting a pronounced immunosuppressive state in the TME. Based on these results, we infer that prognosis-related MRGs drive high M2 macrophage infiltration, leading to an immunosuppressive TME in cervical cancer and, consequently, poorer clinical outcomes. In summary, our M2 macrophage-related predictive model not only serves as a tool for assessing patient prognosis but also provides a basis for evaluating immune responses, thereby offering valuable guidance for the development of individualized therapeutic strategies for cervical cancer.

Our risk scoring model effectively predicts the sensitivity of cervical cancer patients to various chemotherapeutic agents. Notably, the high-risk group exhibited significantly poorer sensitivity to most chemotherapy drugs, which aligns with the suboptimal performance of conventional chemotherapeutic agents in the treatment of advanced cervical cancer. Furthermore, genomic and epigenetic instability have long been recognized as critical drivers of tumor initiation and progression. Previous studies have identified tumor mutational burden (TMB) as a predictive biomarker for immune checkpoint inhibitor (ICI) response, as increased TMB can lead to the generation of immunogenic neoantigens, resulting in multi-antigen exposure and the induction of anti-tumor immune responses[39]. Consequently, across multiple cancer types, higher TMB levels are often associated with superior clinical efficacy of ICIs[40]. Our risk scoring model revealed that the high-risk group exhibited significantly higher gene mutation frequencies and TMB levels. These findings suggest that our risk scoring model holds promise for evaluating the potential efficacy of immunotherapy in cervical cancer treatment, thereby offering a novel perspective for the development of individualized therapeutic strategies for cervical cancer patients.

Although several studies have reported on the prognostic genes identified in our research, the functional roles of these genes in tumors remain relatively underexplored, and their underlying mechanisms and biological significance warrant further investigation. In our subsequent

experimental studies, we observed that PKD2L1 and PILRA were significantly downregulated in cervical cancer. Compared to the control group, overexpression of PKD2L1 or PILRA markedly inhibited the proliferation of cervical cancer cells, promoted apoptosis, and enhanced sensitivity to cisplatin. Furthermore, their overexpression significantly suppressed tumor growth in nude mice and was associated with higher levels of M2 macrophage infiltration. Our findings provide valuable insights into the potential of PKD2L1 and PILRA as novel therapeutic targets for cervical cancer patients.

In summary, our study expands the screening parameters for prognostic prediction in cervical cancer and provides novel transcriptomic-level evidence supporting the immunosuppressive role of M2 macrophages in the cervical cancer microenvironment. However, this study is not without limitations. Although we conducted preliminary validation experiments, the majority of our data were derived from retrospective analyses of existing public databases. As a result, the stability of our risk model requires further validation in large-scale prospective clinical cohorts. Moving forward, we plan to initiate real-world clinical studies to further validate our findings and conduct in vitro and in vivo experiments to elucidate the underlying molecular mechanisms in greater depth.

Conclusion

We have developed a novel MRG-based prognostic model for cervical cancer, which explores the immune landscape associated with M2-like tumor-associated macrophage (TAM)-related genes. This model demonstrates robust predictive value and accuracy for cervical cancer prognosis, holding significant potential to guide clinical decision-making. Furthermore, our study highlights the tumor-suppressive roles of PKD2L1 and PILRA, key components of the model, in cervical cancer, as well as their ability to mitigate cisplatin resistance. These findings provide a theoretical foundation for advancing targeted immunotherapy research in cervical cancer.

Declarations

Funding

This work was supported by the Scientific Research Project of the Health Commission of Hubei Province (Grant No. 2023F044).

Ethics approval and consent to participate

This study was carried out in accordance with the guidelines outlined in the Declaration of Helsinki, as approved by the Medical Ethics Committee of Zhongnan Hospital of Wuhan University (Approval No. 2023066).

Data availability

The publicly available datasets analyzed in this study can be accessed at https://portal.gdc.cancer.gov/ and https://www.ncbi.nlm.nih.gov/.

Conflict of interest

The authors have declared that no conflict of interest exists.

Author contributions

W.Z., J.L., Y.H. were primarily involved in designing experiments. W.Z., J.L. and Y.G. Conducted the bioinformatics analysis. W.Z., M.S., Y.G. and Z.L. performed experiments. X.G. and L.C. analysed and interpreted the data. W.Z. wrote the manuscript with the revision. Y.H. supervised the study. All authors read the final draft and approved the submitted manuscript.

References

[1] Siegel R L, Miller K D, Jemal A. Cancer statistics, 2020[J]. CA Cancer J Clin, 2020, 70(1): 7-30.

[2] Rahangdale L, Mungo C, O'connor S, et al. Human papillomavirus vaccination and cervical cancer risk[J]. Bmj, 2022, 379: e070115.

[3] Garg P, Krishna M, Subbalakshmi A R, et al. Emerging biomarkers and molecular targets for precision medicine in cervical cancer[J]. Biochim Biophys Acta Rev Cancer, 2024, 1879(3): 189106.

[4] Marth C, Landoni F, Mahner S, et al. Cervical cancer: ESMO Clinical Practice Guidelines for diagnosis, treatment and follow-up[J]. Ann Oncol, 2017, 28(suppl_4): iv72-iv83.

[5] Li C, Guo L, Li S, et al. Single-cell transcriptomics reveals the landscape of intra-tumoral heterogeneity and transcriptional activities of ECs in CC[J]. Mol Ther Nucleic Acids, 2021, 24: 682-694.

[6] Wang Y, Wang C, Qiu J, et al. Targeting CD96 overcomes PD-1 blockade resistance by enhancing CD8+ TIL function in cervical cancer[J]. J Immunother Cancer, 2022, 10(3).

[7] Chen S, Wang M, Lu T, et al. JMJD6 in tumor-associated macrophage regulates macrophage polarization and cancer progression via STAT3/IL-10 axis[J]. Oncogene, 2023, 42(37): 2737-2750.

[8] Cohen P A, Jhingran A, Oaknin A, et al. Cervical cancer[J]. Lancet, 2019, 393(10167): 169-182.

[9] Fan G, Gao R, Xie T, et al. DKK1+ tumor cells inhibited the infiltration of CCL19+ fibroblasts and plasma cells contributing to worse immunotherapy response in hepatocellular carcinoma[J]. Cell Death Dis, 2024, 15(11): 797.

[10] Yan X, Zhang S, Jia J, et al. Exosomal MiR-423-3p inhibits macrophage M2 polarization to suppress the malignant progression of cervical cancer[J]. Pathol Res Pract, 2022, 235: 153882.

[11] Hadiloo K, Taremi S, Heidari M, et al. The CAR macrophage cells, a novel generation of chimeric antigen-based approach against solid tumors[J]. Biomark Res, 2023, 11(1): 103.

[12] Coulton A, Murai J, Qian D, et al. Using a pan-cancer atlas to investigate tumour associated macrophages as regulators of immunotherapy response[J]. Nat Commun, 2024, 15(1): 5665.

[13] Xia X, Yang Z, Lu Q, et al. Reshaping the tumor immune microenvironment to improve CAR-T cell-based cancer immunotherapy[J]. Mol Cancer, 2024, 23(1): 175.

[14] Hu Q, Lyon C J, Fletcher J K, et al. Extracellular vesicle activities regulating macrophage- and tissue-mediated injury and repair responses[J]. Acta Pharm Sin B, 2021, 11(6): 1493-1512.

[15] Wang H, Wang X, Zhang X, et al. The promising role of tumor-associated macrophages in the treatment of cancer[J]. Drug Resist Updat, 2024, 73: 101041.

[16] Li W, Wu F, Zhao S, et al. Correlation between PD-1/PD-L1 expression and polarization in tumor-associated macrophages: A key player in tumor immunotherapy[J]. Cytokine Growth Factor Rev, 2022, 67: 49-57.

[17] Liu Y, Zheng H, Gu A M, et al. Identification and Validation of a Metabolism-Related Prognostic Signature Associated with M2 Macrophage Infiltration in Gastric Cancer[J]. Int J Mol Sci, 2023, 24(13).

[18] Newman A M, Steen C B, Liu C L, et al. Determining cell type abundance and expression from bulk tissues with digital cytometry[J]. Nat Biotechnol, 2019, 37(7): 773-782.
[19] Yu G, Wang L G, Han Y, et al. clusterProfiler: an R package for comparing biological themes among gene clusters[J]. Omics, 2012, 16(5): 284-7.
[20] Jiang J, Xu Y, Chen D, et al. Pan-cancer analysis of immune checkpoint receptors and ligands in various cells in the tumor immune microenvironment[J]. Aging (Albany NY), 2024, 16(15): 11683-11728.
[21] Ma Y, Kroemer G. The cancer-immune dialogue in the context of stress[J]. Nat Rev Immunol, 2024, 24(4): 264-281.
[22] Liu Y, Wang Y, Yang Y, et al. Emerging phagocytosis checkpoints in cancer immunotherapy[J]. Signal Transduct Target Ther, 2023, 8(1): 104.
[23] Janjigian Y Y, Shitara K, Moehler M, et al. First-line nivolumab plus chemotherapy versus chemotherapy alone for advanced gastric, gastro-oesophageal junction, and oesophageal adenocarcinoma (CheckMate 649): a randomised, open-label, phase 3 trial[J]. Lancet, 2021, 398(10294): 27-40.
[24] Herbst R S, Arkenau H T, Santana-Davila R, et al. Ramucirumab plus pembrolizumab in patients with previously treated advanced non-small-cell lung cancer, gastro-oesophageal cancer, or urothelial carcinomas (JVDF): a multicohort, non-randomised, open-label, phase 1a/b trial[J]. Lancet Oncol, 2019, 20(8): 1109-1123.
[25] Qiu J, Qu X, Wang Y, et al. Single-Cell Landscape Highlights Heterogenous Microenvironment, Novel Immune Reaction Patterns, Potential Biomarkers and Unique Therapeutic Strategies of Cervical Squamous Carcinoma, Human Papillomavirus-Associated (HPVA) and Non-HPVA Adenocarcinoma[J]. Adv Sci (Weinh), 2023, 10(10): e2204951.
[26] Cao G, Yue J, Ruan Y, et al. Single-cell dissection of cervical cancer reveals key subsets of the tumor immune microenvironment[J]. Embo j, 2023, 42(16): e110757.
[27] Hu A, Sun L, Lin H, et al. Harnessing innate immune pathways for therapeutic advancement in cancer[J]. Signal Transduct Target Ther, 2024, 9(1): 68.
[28] Lin X, Wang F, Chen J, et al. N(6)-methyladenosine modification of CENPK mRNA by ZC3H13 promotes cervical cancer stemness and chemoresistance[J]. Mil Med Res, 2022, 9(1): 19.
[29] Wan Z, Huang H, West R E, 3rd, et al. Overcoming pancreatic cancer immune resistance by codelivery of CCR2 antagonist using a STING-activating gemcitabine-based nanocarrier[J]. Mater Today (Kidlington), 2023, 62: 33-50.
[30] Chen W, Chen M, Hong L, et al. M2-like tumor-associated macrophage-secreted CCL2 facilitates gallbladder cancer stemness and metastasis[J]. Exp Hematol Oncol, 2024, 13(1): 83.
[31] Li R, Zhou R, Wang H, et al. Gut microbiota-stimulated cathepsin K secretion mediates TLR4-dependent M2 macrophage polarization and promotes tumor metastasis in colorectal cancer[J]. Cell Death Differ, 2019, 26(11): 2447-2463.
[32] Bian Z, Wu X, Chen Q, et al. Oct4 activates IL-17A to orchestrate M2 macrophage polarization and cervical cancer metastasis[J]. Cancer Immunol Immunother, 2024, 73(4): 73.
[33] Li J, Cao Y, Liu Y, et al. Multiomics profiling reveals the benefits of gamma-delta (γδ) T lymphocytes for improving the tumor microenvironment, immunotherapy efficacy and prognosis in cervical cancer[J]. J Immunother Cancer, 2024, 12(1).
[34] Qu X, Wang Y, Jiang Q, et al. Interactions of Indoleamine 2,3-dioxygenase-expressing

LAMP3(+) dendritic cells with CD4(+) regulatory T cells and CD8(+) exhausted T cells: synergistically remodeling of the immunosuppressive microenvironment in cervical cancer and therapeutic implications[J]. Cancer Commun (Lond), 2023, 43(11): 1207-1228.
[35] Guo C, Qu X, Tang X, et al. Spatiotemporally deciphering the mysterious mechanism of persistent HPV-induced malignant transition and immune remodelling from HPV-infected normal cervix, precancer to cervical cancer: Integrating single-cell RNA-sequencing and spatial transcriptome[J]. Clin Transl Med, 2023, 13(3): e1219.
[36] Liu Z, Zhu Y, Xu L, et al. Tumor stroma-infiltrating mast cells predict prognosis and adjuvant chemotherapeutic benefits in patients with muscle invasive bladder cancer[J]. Oncoimmunology, 2018, 7(9): e1474317.
[37] Baumeister S H, Freeman G J, Dranoff G, et al. Coinhibitory Pathways in Immunotherapy for Cancer[J]. Annu Rev Immunol, 2016, 34: 539-73.
[38] Zhang J, Dang F, Ren J, et al. Biochemical Aspects of PD-L1 Regulation in Cancer Immunotherapy[J]. Trends Biochem Sci, 2018, 43(12): 1014-1032.
[39] Budczies J, Kazdal D, Menzel M, et al. Tumour mutational burden: clinical utility, challenges and emerging improvements[J]. Nat Rev Clin Oncol, 2024, 21(10): 725-742.
[40] Samstein R M, Lee C H, Shoushtari A N, et al. Tumor mutational load predicts survival after immunotherapy across multiple cancer types[J]. Nat Genet, 2019, 51(2): 202-206.

Supplementary Files

This is a list of supplementary files associated with this preprint. Click to download.

- SupplementaryFigures.docx